Available online at www.sciencedirect.com
ScienceDirect
Planetary and Space Science 56 (2008) 1596–1606
Planetary and Space Science
www.elsevier.com/locate/pss

Geysers of Enceladus: Quantitative analysis of qualitative models

Nikolai V. Brilliantov[a,*], Jürgen Schmidt[b], Frank Spahn[b]

[a]Department of Mathematics, University of Leicester, University Road, Leicester LE1 7RH, UK
[b]Institute of Physics, University of Potsdam, Am Neuen Palais 10, 14469 Potsdam, Germany

Received 12 June 2008; accepted 13 June 2008
Available online 1 July 2008

Abstract

Aspects of two qualitative models of Enceladus' dust plume—the so-called "Cold Faithful" [Porco, C.C., et al., 2006. Cassini observes the active south pole of Enceladus. Science 311, 1393–1401; Ingersoll, A.P., et al., 2006. Models of the Enceladus plumes. In: Bulletin of the American Astronomical Society, vol. 38, p. 508] and "Frigid Faithful" [Kieffer, S.W., et al., 2006. A clathrate reservoir hypothesis for Enceladus' south polar plume. Science 314, 1764; Gioia, G., et al., 2007. Unified model of tectonics and heat transport in a Frigid Enceladus. Proc. Natl. Acad. Sci. 104, 13578–13591] models—are analyzed quantitatively. The former model assumes an explosive boiling of subsurface liquid water, when pressure exerted by the ice crust is suddenly released due to an opening crack. In the latter model the existence of a deep shell of clathrates below Enceladus' south pole is conjectured; clathrates can decompose explosively when exposed to vacuum through a fracture in the outer icy shell. For the Cold Faithful model we estimate the maximal velocity of ice grains, originating from water splashing in explosive boiling. We find that for water near the triple point this velocity is far too small to explain the observed plume properties. For the Frigid Faithful model we consider the problem of momentum transfer from gas to ice particles. It arises since any change in the direction of the gas flow in the cracks of the shell requires re-acceleration of the entrained grains. While this effect may explain the observed speed difference of gas and grains if the gas evaporates from triple point temperature (273.15 K) [Schmidt, J., et al., 2008. Formation of Enceladus dust plume. Nature 451, 685], the low temperatures of the Frigid Faithful model ($\sim$140−170 K) imply a too dilute vapor to support the observed high particle fluxes in Enceladus' plume.

Keywords: Enceladus plume; Cold Faithful model; Frigid Faithful model; Icy satellites; Explosive boiling

1. Introduction

In 2004 the Cassini spacecraft entered its orbit around Saturn, opening an era of intense studies of the gaseous giant planet, its magnificent rings and satellites. The small (500 km in diameter) icy moon Enceladus was in the focus of observations because of its role for the origin and the sustainment of the dusty Saturnian E ring. From pre-Cassini spacecraft observations (Showalter et al., 1991), the Hubble Space Telescope (Nicholson et al., 1996) and KECK infrared observations (De Pater et al., 1996, 2004) it was clear that Enceladus is likely the main source of the E ring. Namely, the minimal vertical extent and the maximum particle number density of the E ring were found near the orbit of Enceladus. Dynamical models for grains ejected from Enceladus successfully reproduced the basic properties of the E ring (Horányi et al., 1992; Juhász and Horányi, 2002). Moreover, the rather narrow size distribution of the E ring (Showalter et al., 1991; Nicholson et al., 1996) and the unusual surface properties of Enceladus—a very high albedo and a heterogeneous distribution of craters, indicating surface regions of very different age—lead to speculations about geophysical activities in form of cryo-volcanism or geysers at Enceladus (Haff et al., 1983; Showalter et al., 1991). The activity of Enceladus was confirmed the Cassini observations in a series of flybys (Dougherty et al., 2006; Spencer et al., 2006; Porco et al., 2006; Spahn et al., 2006; Waite et al., 2006; Hansen et al., 2006).

It turned out that Enceladus possesses an unusually warm south pole which is characterized by a geologically young surface. The heat (at least as high as 140 K, compared to expected 70 K) is concentrated along the

*Corresponding author. Tel.: +44 116 2522521; fax: +44 116 2523915.
E-mail address: nbrillia@agnld.uni-potsdam.de (N.V. Brilliantov).

0032-0633/$ - see front matter
doi:10.1016/j.pss.2008.06.007

"tiger-stripes" (Spencer et al., 2006), a system of four parallel cracks in the ice crust of the satellite. Gas and entrained icy grains emerge from localized sources (Spitale and Porco, 2007) on the "tiger stripes" forming the large dust and gas plume towering the south-polar terrain (SPT; Porco et al., 2006). Furthermore, Cassini observations indicate that the icy grains are decoupled from the gas in the plume (Ingersoll et al., 2006). This requires a subsurface creation and acceleration of dust grains which later make up the dust plume and eventually populate the E ring. The new findings of the Cassini mission suggest a hot interior of Enceladus and the presence of liquid water (Matson et al., 2007; Collins and Goodman, 2007).

In our study we focus on the question of origin and acceleration of ice grains, which form the dust part of the plume. We quantitatively study aspects of two recent models of the plume, termed as "Cold Faithful" (Porco et al., 2006; Ingersoll et al., 2006) and "Frigid Faithful" (Kieffer et al., 2006; Gioia et al., 2007) models. We show that while both models give an alternative explanation of the origin of the dust plume, one encounters difficulties when making quantitative estimates.

The "Cold Faithful" model assumes the presence of liquid-filled cavities, or pockets in the ice shell of the moon, presumably at the water triple point (about 273.16 K) and located at a depth of about 10 m (Porco et al., 2006). The plumes erupt when cracks in the ice shell (perhaps opened by tectonic processes) cause the sudden exposition of liquid water to vacuum. The water starts to boil violently producing vapor and splashes, which freeze and form eventually a gas flux with entrained ice particles.

In the alternative "Frigid Faithful" model (Kieffer et al., 2006) it is assumed that Enceladus has a shell of H_2O–CO_2 ice on top of another shell composed of H_2O ice and H_2O clathrates containing CO_2, CH_4, and N_2. The composition of the gas plume (Waite et al., 2006) in this model therefore reflects the composition of the clathrate shell. When a crack in the ice crust propagates due to tectonic activity down to the clathrate-rich shell and exposes its material to vacuum, the clathrates start to decompose. This process may occur explosively, exposing more and more clathrate surface to vacuum. The model then requires that the eruptions can proceed as a self-sustained phenomenon. The gas mixture produced in the clathrate dissociation contains water vapor (the main component) and the above mentioned volatile gases, which are observed in the plume (Waite et al., 2006). Due to the explosive nature of the clathrate decomposition the gas flux is assumed to carry small ice debris; additionally, the ice grains might originate from water vapor condensation into ice (Kieffer et al., 2006). The clathrate decomposition may occur at temperatures as low as ≈ 133 K (Gioia et al., 2007).

In the remainder of the paper we develop quantitative estimates for the dynamics of the dust grains forming the plume as these follow from both models.

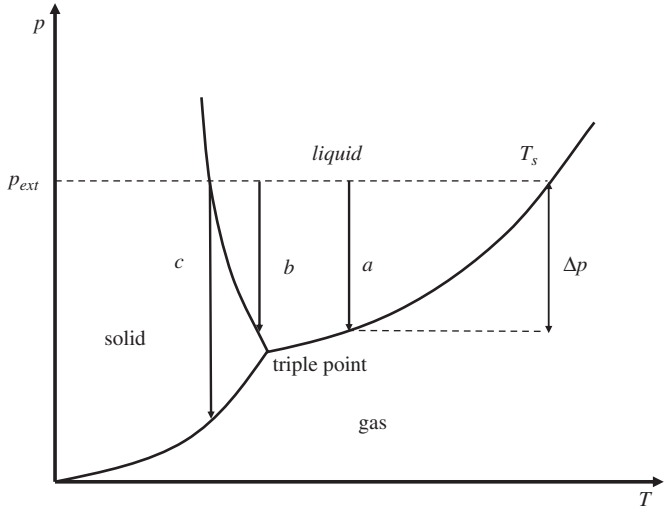

Fig. 1. The schematic phase diagram of water. Only a part of the complete diagram, around the triple point ($T_{t.p.}$, $p_{t.p.}$), is shown. Note the negative slope of the liquid–solid coexistence curve. The initial location of the system is on the dashed line, with the external pressure equal p_{ext}. The same pressure would have saturated vapor at temperature T_s. When the external pressure is suddenly released, a few different scenarios of the system evolution are possible: for $T > T_{t.p.}$ it evolves through the liquid–gas coexistence curve, case (a). For $T < T_{t.p.}$ the system evolution takes place either through the liquid–solid coexistence curve, case (b), or through the solid–gas coexistence curve, case (c). Only for the cases (a) and (c) the release of the external pressure causes an abundant production of vapor.

2. Analysis of the "Cold Faithful" model

In the "Cold Faithful" model it is argued that a phase transition from liquid water into ice and vapor, in the proportion which follows from the conservation of energy, leads to a significant increase of the system volume. This may produce a fast gas flux carrying entrained ice particles (Porco et al., 2006; Ingersoll et al., 2006). These estimates were based on thermodynamic arguments. Here we address the problem in more detail, taking into account the microscopic mechanism of the process and its kinetics.

Let us consider liquid water at some external pressure p_{ext}, which suddenly drops to zero. As it is clear from the phase diagram, Fig. 1, the final outcome is an infinitely dilute gas.[1] However, when the system evolves to this state, it unavoidably reaches the coexistence curve (Fig. 1). Here the most intensive vaporization during the liquid–gas phase transition takes place. If the temperature T of the system is larger than that of the triple point, $T_{t.p.}$, it evolves through the liquid–gas coexistence curve (Fig. 1, path "a"). Contrary, for $T < T_{t.p.}$, the system first attains the liquid–solid coexistence and then achieves the solid–gas curve (Fig. 1, path "b"). If the system starts from liquid–solid equilibrium, it evolves directly to the gas–solid coexistence curve (Fig. 1, path "c"). While during the phase

[1]The evaporation of the solid phase critically slows down at the low surface temperatures, hence the icy bodies in the Saturnian system (with $T < 70$ K) are stable on the time scale of interest.

transition at the liquid–solid curve no gas is produced, the vapor production is abundant on the gas–solid path. In what follows we consider these two cases separately.

2.1. Thermodynamic approach to the explosive boiling

We start from the thermodynamic approach, which is being rather simple, allows to get the upper-limit estimates for the velocity of water droplets, produced by the explosive boiling. Thermodynamic approach has been also applied for the analysis of geysers on Titan (Lorenz, 2002). First we consider the basic physics of the phenomenon and address the case of $T > T_{\text{t.p.}}$, when after the release of the external pressure p_{ext} the system drops to the liquid–vapor coexistence curve (Fig. 1, path "a"). In this case the liquid phase becomes unstable, while the vapor is stable, so that the transformation of the unstable phase (water) into the stable phase (gas) takes place. Thermodynamically speaking, this process occurs because the chemical potential of vapor, $\mu_{\text{v}}(T, p_{\text{v}})$ ($p_{\text{v}} = p_{\text{v}}^{\text{l.g.}}(T)$ is the saturated vapor pressure at temperature T on the liquid–gas coexistence curve), is lower than the chemical potential of water $\mu_{\text{w}}(T, p_{\text{ext}})$, initially prepared at pressure p_{ext}. Since the systems tend to the minimum of the Gibbs free energy G and the chemical potential is just the Gibbs potential per molecule, the above transformation is favorable. However, if the gaseous phase arises in the bulk of the liquid in form of bubbles (which implies boiling) the Gibbs free energy acquires an additional positive contribution due to the interphase boundary. Let s_{v} be the total surface of all bubbles and σ be the gas–liquid surface tension; then this contribution reads, $s_{\text{v}}\sigma$. The formation of surface in thermodynamically unfavorable, hence the "negative gain" of the Gibbs free energy, $(\mu_{\text{v}} - \mu_{\text{w}})N$ related to the transition of N molecules from the liquid to the vapor phase, should exceed the "positive loss" due to the surface term $s_{\text{v}}\sigma$. Since N grows with the bubble radius R as $N \sim R^3$, while $s_{\text{v}} \sim R^2$, this is only possible if bubbles are large enough. Moreover, there exist a critical radius, R_{cr}, such that bubbles with radius smaller than R_{cr}, shrink, while those with $R > R_{\text{cr}}$ unlimitedly grow. In principle bubbles uniformly originate in a bulk of a pure metastable liquid due to thermal fluctuations. The lower the liquid temperature and the larger the bubble, the less probable is the respectivefluctuation. In this case the rate γ at which critical bubbles arise is given by the homogeneous nucleation theory. Once formed, a bubble with $R > R_{\text{cr}}$, starts to grow and push the surrounding liquid outwards; this causes the increase of the total volume V of the system. The growth rate $\dot{R}$ is described by the hydrodynamic equation and depends on the vapor pressure inside the bubble, the external pressure, liquid density, and viscosity. Hence, the growth rate $\dot{V}$ is determined by the homogeneous nucleation rate γ and the bubble growth rate $\dot{R}$.

Naturally, the increase of the system volume $V = V_0 + V_{\text{v}}$, where V_0 is the initial liquid volume and V_{v} is the vapor volume, will cause a mechanical acceleration of the liquid. Let water start to boil in a crack in the icy shell of a cross-section S and boiling take place in a column of height L. Then the increase of the volume $\Delta V = V_{\text{v}}$ implies the increase of the column height $\Delta V = \Delta L S$. Correspondingly, the velocity u_0 of the uppermost part of water in the slit reads

$$u_0(t) = \frac{\mathrm{d}\Delta L}{\mathrm{d}t} = \frac{1}{S}\frac{\mathrm{d}\Delta V}{\mathrm{d}t} = \frac{\dot{V}_{\text{v}}}{S}, \tag{1}$$

hence the water speed is determined by the rate $\dot{V}_{\text{v}}$.

One may ask, to what extent can the volume V increase, or equivalently, how large can be the volume increment $\Delta V = V_{\text{v}}$? Eventually, when all liquid of density ρ_{w} transforms into vapor of density ρ_{v}, the system volume becomes $\rho_{\text{w}}/\rho_{\text{v}}$ times larger than the initial liquid volume V_0. For the case of interest the factor of $\rho_{\text{w}}/\rho_{\text{v}}$ may be as large as $10^4 - 10^6$. It is expected that at the intermediate stage of this transformation a spray will be formed, so that the expanding into vacuum vapor will entrain small water droplets.

Here we address the case of explosive boiling, which gives rise to the maximum velocity of the water column. In this case bubbles coalesce much faster than they flow upward in the liquid, due to the small buoyancy in the weak gravity field of Enceladus.

When the vapor bubbles grow and coalesce in the bulk, the fraction of vapor increases, the liquid keeps its integrity only up to a threshold, which is called percolation threshold. According to the "physical" definition (apart from the mathematical strictness), the percolation of some guest substance inside a host body occurs, when one can find a path through the system which remains within the guest part (e.g. Grimmett, 1989). In application to our system, at the percolation threshold a spanning vapor cluster arises, so that the vapor can find pathways to the surface and escape the liquid without carrying it along. Beyond this point rupture of the liquid occurs and droplets are formed. In principle, they may be further accelerated by the vapor flow, but much less efficiently. Hence $u_0(t_{\text{p}})$, where t_{p} is the percolation time, gives a good estimate for the maximal droplet velocity, $u_{\max} \simeq u_0(t_{\text{p}})$, accelerated to space due to explosive boiling. In the case of interest we have a percolation transition of vapor bubbles which are assumed to be spherical with some distribution of radii, determined by the nucleation and growth rates. The percolation threshold generally depends on the shape and size distribution of percolating objects and is given by the relation $V_{\text{guest}} = \zeta V_{\text{host}}$, where V_{host} and V_{guest} are, respectively, the volume of the host and the guest component and ζ is a constant of order unity. In our case $V_{\text{guest}} = V_{\text{v}}(t_{\text{p}})$ is the volume of the vapor component at the time of percolation, $V_{\text{host}} = V_0$, and to obtain an order of magnitude estimate for u_{max} we approximate the percolation condition by

$$V_{\text{v}}(t_{\text{p}}) = V_0. \tag{2}$$

Thus, to find the maximal droplet velocity $u_{\max} \simeq u_0(t_p)$ one needs to determine the evolution of $\Delta V(t) = V_v(t)$, to determine the percolation time from condition (2) and finally to obtain $u_0(t_p) = \dot{V}(t_p)/S$.

Here, we develop a simple expression for an upper limit of the speed of droplets at the percolation point, using simple thermodynamic arguments, describing the (reversible) phase transition at constant pressure and temperature (Landau and Lifshitz, 1980; Debenedetti, 1996; Zettlemoyer, 1969). Elements of a kinetic theory of boiling from homogeneous nucleation theory and the growth of bubbles are given in Section 2.2. The maximal work ΔW done by the system during the phase transformation is given by

$$-\Delta W = \Delta G = (\mu_v - \mu_w)N + \sigma s_v. \tag{3}$$

The number of molecules N in the vapor phase of volume $V_v(t_p) = V_0$ reads

$$N = \frac{\rho_v V_0}{m_0} = \rho_w V_0 \frac{\rho_v}{\rho_w m_0} = \frac{\rho_v}{\rho_w}\frac{M}{m_0}, \tag{4}$$

where m_0 is the mass of a water molecule, $\rho_v = \rho_v(T) = m_0 p_v^{l.g.}(T)/k_B T$ is the saturated vapor density at temperature T, which is assumed to be an ideal gas and k_B is the Boltzmann constant; $M = \rho_w V_0$ is the mass of the water column before the expansion. The mechanical work ΔW is the sum of the kinetic energy E_{kin} of the water column, where the uppermost part moves with the velocity $u_{\max}$, and the potential energy, E_{pot}, due to shift of the center mass of the column in the Enceladus gravity.

E_{kin} may be estimated as follows. For simplicity we neglect the impact of the hydrostatic pressure on the nucleation and growth and assume that these processes take place uniformly in the water column, which implies its uniform expansion. Hence, if the velocity at the top of the column of height L is $u_{\max}$ and at the bottom it is zero, the velocity at the depth h from the top is given by

$$u(h) = u_{\max}(1 - h/L). \tag{5}$$

Then the kinetic energy of water column in the slit is

$$E_{kin} = \frac{1}{2}\int_0^L S\rho u(h)^2\,\mathrm{d}h = \frac{1}{6}(\rho SL)u_{\max}^2 = \frac{1}{6}Mu_{\max}^2, \tag{6}$$

where $\rho = M/SL$ is the density of the expanded water column of length L.

To estimate E_{pot} we notice that at the percolation point the total volume of the column, $V = V_0 + V_v = 2V_0$, is twice the initial one and therefore its length is also twice the initial length L_0. Therefore, the center of mass of the column, located at the middle for the uniform expansion, shifts by $(2L_0)/2 - L_0/2 = L_0/2$ upwards, which yields

$$E_{pot} = MgL_0/2, \tag{7}$$

where g is the gravitational acceleration on Enceladus (g is about 86 times smaller than on Earth). Substituting $\Delta W = E_{kin} + E_{pot}$ into Eq. (3) with E_{kin} and E_{pot} given by Eqs. (6) and (7) and using Eq. (4) for N, we recast this equation into the form

$$\frac{Mu_{\max}^2}{6} + \frac{MgL_0}{2} = \Delta\mu\frac{\rho_v}{\rho_w}\frac{M}{m_0} - \sigma s_v, \tag{8}$$

where $\Delta\mu = (\mu_w - \mu_v)$.

While L_0 may be estimated from the balance between the hydrostatic and saturated vapor pressure (see the discussion below), to estimate the total surface of the vapor–liquid interface s_v one needs to know the details of the nucleation and growth kinetics of vapor bubbles, which is beyond the scope of this paper. Still for the upper-limit estimates one can neglect the surface term in Eq. (8), moreover, the potential energy term $MgL_0/2$ may be also neglected due to the weak Enceladus gravity. As a result we obtain from the above equation the upper-limit velocity acquired by the water droplets due to the explosive boiling:

$$u_{\max} = \sqrt{6\left(\frac{\Delta\mu}{m_0}\right)\left(\frac{\rho_v(T)}{\rho_w(T)}\right)}. \tag{9}$$

Taking into account that for a constant temperature $\mathrm{d}\mu = v\,\mathrm{d}p$, where in the case of interest $v = v_w = m_0/\rho_w$ is the volume per molecule in water and p is the pressure (Landau and Lifshitz, 1980), we write for the chemical potential of water:

$$\mu_w(p_{ext}, T) = \mu_v(p_v, T) + \int_{p_v}^{p_{ext}} v_w(p)\,\mathrm{d}p. \tag{10}$$

Here, we use the fact that on the liquid–vapor coexistence curve the water and vapor chemical potentials are equal. If we further take into account that liquid is almost incompressible at the temperatures of interest we obtain

$$\Delta\mu \simeq \left(\frac{m_0}{\rho_w(T)}\right)(p_{ext} - p_v^{l.g.}(T)) = k_B T\left(\frac{\rho_v^{l.g.}}{\rho_w}\right)\left(\frac{p_{ext}}{p_v^{l.g.}(T)} - 1\right), \tag{11}$$

where we again employ the ideal-gas relation $p_v^{l.g.} = k_B T\rho_v/m_0$. Substituting Eq. (11) into Eq. (9) we finally obtain for the maximal velocity:

$$u_{\max} = \langle w_g\rangle\left(\frac{\rho_v^{l.g.}}{\rho_w}\right)\sqrt{\frac{3\pi}{4}\left(\frac{p_{ext}}{p_v^{l.g.}(T)} - 1\right)}, \tag{12}$$

with $\langle w_g\rangle = (8k_B T/\pi m_0)^{1/2}$ being the average molecular speed of the gas at temperature T.

Similar estimates are possible for the case when the system was initially in equilibrium at the liquid–solid coexistence curve (Fig. 1c). Here the transition of the compressed water into a gas–solid mixture takes place so that simultaneously the vapor and ice phase form in the bulk of the liquid. If we again assume explosive boiling, which provides the maximum acceleration for the water droplets, we conclude that this still happens when the vapor phase forms a system spanning percolation cluster, that is for $V_v \approx V_0$. The thermodynamic equation,

analogous to (3) reads now

$$-\Delta W = \Delta G = (\mu_v - \mu_w)N_1 + (\mu_{ice} - \mu_w)N_2 + \sigma s_v + \sigma_{i.w.}s_{i.w.} + \sigma_{i.v.}s_{i.v.}. \quad (13)$$

Note that here $\mu_{ice} = \mu_v$, that is, the chemical potentials of ice and vapor are equal on the *solid–gas* coexistence curve. N_1 and N_2 are the number of molecules in vapor and ice phase, respectively. $\sigma_{i.w.}$ and $s_{i.w.}$ in Eq. (13) are the surface tension and the total area of the ice–water interface, while $\sigma_{i.v.}$ and $s_{i.v.}$ are the corresponding quantities for the ice–vapor interface. The work of the system, ΔW, may be estimated just in the same way as it has been done previously, while for the chemical potential of the compressed water one can write

$$\mu_w(p_{ext}, T) \simeq \mu_{ice}(p_v, T) + \left(\frac{m_0}{\rho_{ice}(T)}\right)(p_{ext} - p_v^{s.g.}(T)). \quad (14)$$

Here we again use the relation $d\mu = v\,dp$ with $v = v_{ice} = m_0/\rho_{ice}$, neglecting the change of the ice density and take into account that the chemical potential of water on the liquid–solid coexistence curve (the initial stage of the system, path "c" in Fig. 1) and of ice are equal. Note also that $p_v^{s.g.}(T)$ in the above equation refers to the equilibrium vapor pressure on the *solid–gas* coexistence curve.

To find N_1 we can use Eq. (4), which yields $N_1 = (\rho_v^{s.g.}/\rho_w)(M/m_0)$, with the saturated vapor density on the solid–gas coexistence curve, $\rho_v^{s.g.} = m_0 p_v^{s.g.}(T)/k_B T$. To find N_2 we assume that for the explosive boiling the local energy balance is fulfilled, that is, the energy released in solidification is equal to the energy consumed in evaporation. With the specific heat of melting B_{melt} and evaporation, B_{ev}, per molecule, this condition yields

$$B_{melt}N_2 = B_{ev}N_1. \quad (15)$$

Introducing the specific heats per unit mass, $Q_{melt} = B_{melt}/m_0$ and $Q_{ev} = B_{ev}/m_0$ we obtain

$$N_2 = N_1(Q_{ev}/Q_{melt}). \quad (16)$$

Note that the local energy balance, Eq. (15), is an additional assumption of our theory, since the maximal isothermal work ΔW implies that the temperature is kept uniform and constant by processes of thermal conductivity, which are fast enough. Application of condition (15) guarantees, however, that the thermodynamic estimates will not be invalidated by the limited speed of the heat transfer.

If we again neglect the potential energy E_{pot} in the weak Enceladus gravity and all surface contributions in the Gibbs free energy, we obtain from Eq. (13) using Eqs. (16), (14) and (6):

$$u_{max} = \langle w_g \rangle \left(\frac{\rho_v^{s.g.}}{\rho_w}\right)\sqrt{\frac{3\pi}{4}\left(\frac{\rho_w}{\rho_{ice}}\right)\left(1 + \frac{Q_{ev}}{Q_{melt}}\right)\left(\frac{p_{ext}}{p_v^{s.g.}(T)} - 1\right)}. \quad (17)$$

To find the maximal velocities given by Eqs. (12) and (17), one needs to know the saturated vapor pressure on the liquid–gas and solid–gas coexistence curves. These are given by the following empirical equations (Peeters et al., 2002):

$$p_v^{l.g.}(T) = A_v \exp[-a_v \log(T/T_0) - b_v(1/T - 1/T_0)] \quad (18)$$

for the liquid–gas coexistence, with the constants $A_v = 610.8\,\text{Pa}$, $a_v = 5.1421$, $b_v = 6828.77\,\text{K}$ and $T_0 = 273.15\,\text{K}$, and

$$p_v^{s.g.}(T) = \exp[-(d_v/T + e_v)\log(10)] \quad (19)$$

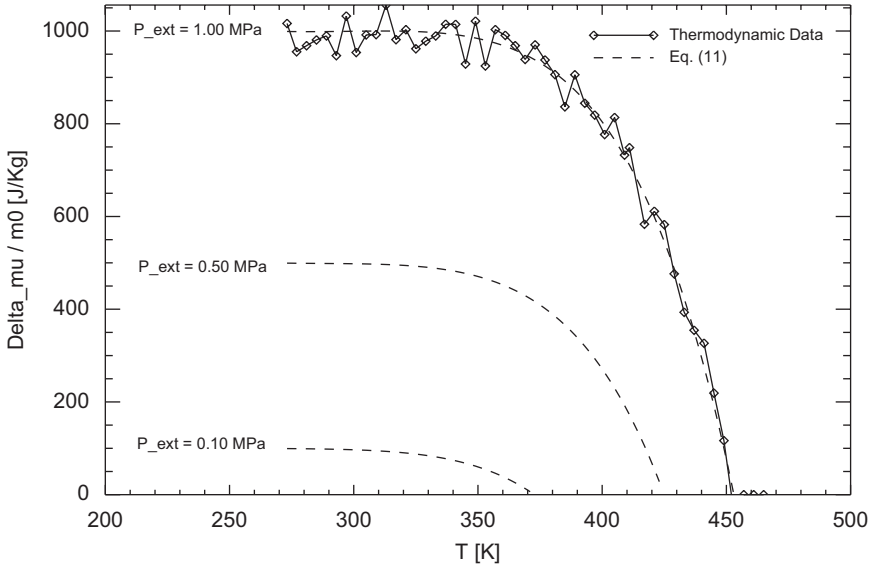

Fig. 2. Temperature dependence of the chemical potential difference per unit mass, $\Delta\mu/m_0$, of the compressed water and of water on the liquid–gas coexistence curve. The compression is quantified by the initial external pressure p_{ext}, which is related to the hydrostatic pressure due to the ice shell of height H as $p_{ext} = \rho_{ice}gH$. The pressure on the coexistence curve is given by Eq. (18). Diamond symbols are obtained from thermodynamic data (Lemmon et al., 2005) and Eq. (11) is shown as a dashed line. Note that the simple relation (11) provides a quite satisfactory accuracy for the value of $\Delta\mu/m_0$.

in Pa for the solid–gas branch, with $d_v = 2663.5\,\mathrm{K}$ and $e_v = 12.537$.

Before computation of the maximal velocity, given by Eqs. (12) and (17), we check the accuracy of the chemical potential difference, as estimated from Eq. (11). In Fig. 2 this difference of the chemical potentials of the compressed water and water in equilibrium with saturated vapor is shown, as the function of temperature for different compressions. These are quantified by the external pressure p_{ext}, related to the hydrostatic pressure of the ice shell of height H as $p_{ext} = \rho_{ice} g H$. In this figure the predictions of the simple relation (11) are compared for $p_{ext} = 1\,\mathrm{MPa}$ to the direct computation of $\Delta\mu$ from thermodynamic data for water at different temperatures (Lemmon et al., 2005). A similarly good accuracy of Eq. (11) is found for other values of the external pressure.

In Fig. 3 we show the dependence of the maximal velocity of water droplets after explosive boiling as a function of temperature for different values of the initial external pressure, as it follows from Eq. (12) for temperatures above the triple point, $T > T_{t.p.}$ and from Eq. (17) for temperatures below $T_{t.p.}$. For the latter case the external pressure p_{ext} is to be taken as the equilibrium pressure on the solid–gas coexistence curve (path "c" in Fig. 1). For a reasonable height of the ice shell, $H < 10^4\,\mathrm{m}$, which correspond to the external pressure $p_{ext} < 1\,\mathrm{MPa}$, the water temperature cannot drop below the triple point for more than a fraction of 1 K. This enables the use of the Clausius–Clapeyron relation (Landau and Lifshitz, 1980), that yields, $p_{ext} = p_{t.p.} + (Q_{melt}/T_{t.p.}\Delta V)(T - T_{t.p.})$, where $p_{t.p.}$ is the triple point pressure and ΔV is the difference of the specific volume of water and ice at the triple point, equal to 0.083 of the specific volume of ice (Lemmon et al., 2005).

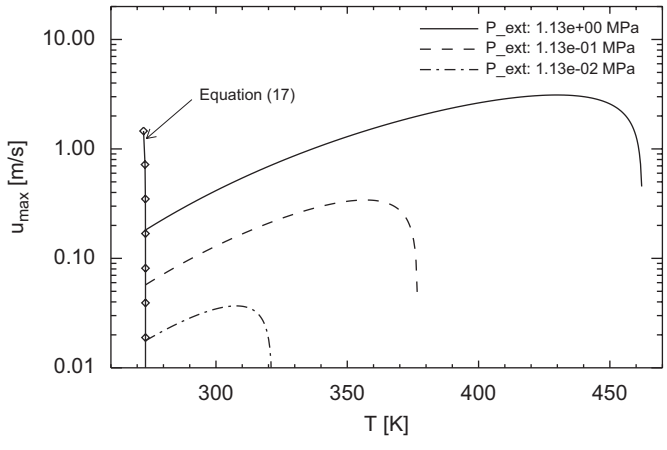

Fig. 3. Maximum velocity of the water droplets in the explosive boiling as a function of temperature, given by the thermodynamic approach for different values of the external pressure p_{ext}. The right curves refer to the case of $T > T_{t.p.}$, described by Eq. (12), while the curve on the left is according to Eq. (17), for temperatures below the triple point temperature, $T_{t.p.}$. The external pressures for the right curves correspond (from top to bottom) to 10.8 km, 1.08 km and 108 m height of the ice shell.

Note the very steep increase of maximal velocity with the decrease of temperature (or the increase of pressure p_{ext}) for the case of $T < T_{t.p.}$. This behavior is caused by the very steep dependence of the pressure on temperature on the liquid–solid coexistence curve. For the case of $T > T_{t.p.}$ the maximal velocity assumes a maximum for a certain temperature. Namely, for larger temperatures the tendency of $\Delta\mu$ to increase with temperature (see Eqs. (9) and (11)) is counterbalanced, and eventually dominated, by the effect of the saturated vapor pressure, which leads to the decrease of $\Delta\mu$ (see Eq. (11)). As it follows from Fig. 3, the maximal velocity cannot exceed 10 m/s, which is far below the escape velocity for Enceladus.

2.2. Elements of the kinetic theory of the explosive boiling

In the previous section we made thermodynamic estimates for the maximal velocity acquired by water droplets in the explosive boiling. Neither the time scale of the process nor its microscopic kinetics have been addressed. Now we consider this phenomenon in more detail. As it has been already noted, the microscopic kinetics of boiling is determined by the nucleation rate γ and the growth rate $\dot{R}$ of a bubble. Although involved theories for these quantities exist, we exploit here the most simple ones. According to the classical nucleation theory, the homogeneous nucleation rate of vapor bubbles in metastable liquid reads (e.g. Blander and Katz, 1975; Lubetkin, 2003):

$$\gamma = \frac{\rho_w}{m_0}\left(\frac{2\sigma}{\pi m_0}\right)^{1/2} \exp\left(-\frac{16\pi}{3}\frac{\sigma^3(1-2q)}{k_B T \Delta\mu^2 (\rho_v(T)/m_0)^2}\right). \quad (20)$$

Here γ gives the number of critical bubbles which nucleate per unit time in a unit volume of liquid and $q = 0$ in the classical theory. Unfortunately, the straightforward application of the classical theory does not even qualitatively agree with experiments, especially for temperatures, not close to the critical point (e.g. Lubetkin, 2003). To improve the predictions of the classical theory and bring it into agreement with observations, an empirical correction factor $(1 - 2q)$ with q close to $\frac{1}{2}$ has been introduced (Delale et al., 2003b). Although improved theories of the homogeneous nucleation have been proposed, which take into account the non-equilibrium nature of the bubble formation (e.g. Li et al., 2005; Kagan, 1960), here we perform the analysis using the more simple theory that employs the phenomenological modification of the nucleation rate (Delale et al. 2003a, b).

The growth kinetics of a vapor bubble is governed by the generalized Rayleigh–Plesset equation (Brennen, 1995; Plesset and Prosperetti, 1977; Alehossein and Quin, 2007), which we use in the following form:

$$\rho_w R\ddot{R} + \frac{3}{2}\rho_w \dot{R}^2 + \frac{4\eta}{R}\dot{R} = p. \quad (21)$$

Here η is the dynamic shear viscosity and we take into account that the pressure at infinite distance from the bubble is zero, $p_\infty = 0$. To find the pressure p in the right-hand side of Eq. (21), which drives the bubble expansion, we use Eq. (3) for a single bubble and write $\Delta W = \mathrm{d}W$ and $\Delta G = \mathrm{d}G$ as

$$\mathrm{d}W = p\,\mathrm{d}V = p\,\mathrm{d}(4\pi R^3/3),$$

$$\mathrm{d}G = -\Delta\mu\,\mathrm{d}(4\pi R^3\rho_\mathrm{v}/3m_0 + 4\pi\sigma R^2), \tag{22}$$

which yields

$$p = \Delta\mu(\rho_\mathrm{v}/m_0) - \frac{2\sigma}{R} = \Delta p_\mathrm{s} - \frac{2\sigma}{R}, \tag{23}$$

where $\Delta p_\mathrm{s} = \Delta\mu(\rho_\mathrm{v}/m_0)$. The bubble can grow only if $p>0$, while for $p<0$ it shrinks. From Eq. (23) we obtain for $p = 0$ the radius of the critical bubble:

$$R_\mathrm{cr} = \frac{2\sigma}{\Delta\mu(\rho_\mathrm{v}/m_0)} = \frac{2\sigma}{\Delta p_\mathrm{s}}. \tag{24}$$

In Eq. (21) we neglect the inertial effects due to the mass transport across the boundary caused by evaporation (Brennen, 1995). We stress, however, that this does not exclude the mass transfer through the bubble boundary, only the acceleration due to evaporation in the bubble is assumed to be negligible. For simplicity we also neglect the temperature gradient and the heat flux from the bulk of the water to the bubble surface (e.g. Li et al., 2005; Kagan, 1960), that is, we assume that the process is isothermal. For the explosive boiling addressed here, the regime of $R \gg R_\mathrm{cr}$ is the most relevant one. Since the temperature gradient, and thus the temperature difference decreases with the bubble radius (Li et al., 2005), we believe that neglecting the heat flux for the regime of interest does not entail a significant error.

Solving Eq. (21) for $R(t)$, we can determine the increment ΔV of a liquid volume at time t after the pressure drop,

$$\Delta V(t) = V_\mathrm{v}(t) = \int_0^t \frac{4}{3}\pi R^3(t-t')\gamma V_0\,\mathrm{d}t', \tag{25}$$

where $\gamma V_0\,\mathrm{d}t'$ gives the number of bubbles nucleated in the volume V_0 during a short time interval $(t', t'+\mathrm{d}t')$, while the factor $(\frac{4}{3})\pi R^3(t-t')$ gives the volume of such bubbles at time t. Using Eq. (1) together with $V_0 = L_0 S$, we write for the velocity of the uppermost layer in the water column,

$$u_0(t) = \frac{4}{3}\pi\gamma R_\mathrm{cr}^3 L_0 + L_0\int_0^t 4\pi R^2(t-t')\dot{R}(t-t')\gamma\,\mathrm{d}t', \tag{26}$$

where we take into account that the bubble starts to grow from the critical radius R_cr.

To estimate the column height L_0 we notice that even after the release of the external pressure the liquid is still subjected to the hydrostatic pressure, $\rho_\mathrm{w}gh$, where h is the depth from the surface. Since the external hydrostatic pressure reduces the pressure difference Δp_s by $\rho_\mathrm{w}gh$, the critical radius is depth dependent, $R_\mathrm{cr} = 2\sigma/(\Delta p_\mathrm{s} - \rho_\mathrm{w}gh)$. This shows that the maximal depth $h = L_0$, below which bubbles cannot grow is

$$L_0 = \frac{\Delta p_\mathrm{s}}{\rho_\mathrm{w}g} = \frac{\Delta\mu}{m_0 g}\frac{\rho_\mathrm{v}}{\rho_\mathrm{w}}. \tag{27}$$

For simplicity we ignore in what follows the depth dependence of R_cr, that is, we approximate $R_\mathrm{cr} = R_\mathrm{cr}(h=0)$.

From Eq. (25) and the condition of percolation, $V_\mathrm{v}(t_\mathrm{p}) = V_0$, we obtain an equation for the percolation time t_p:

$$\int_0^{t_\mathrm{p}} \frac{4}{3}\pi R^3(t_\mathrm{p}-t')\gamma\,\mathrm{d}t' = 1. \tag{28}$$

Solving this equation we find t_p and finally arrive to the expression for the maximal velocity which follows from Eq. (26),

$$u_\mathrm{max} = 4\pi\gamma L_0\left(\frac{1}{3}R_\mathrm{cr}^3 + \int_0^{t_p} R^2(t')\dot{R}(t')\,\mathrm{d}t'\right), \tag{29}$$

where $R(t)$ is the solution of Eqs. (21) and (23), while L_0 and γ are given, respectively, by Eqs. (27) and (20).

Analytical results can be obtained for the case of $R/R_\mathrm{cr} \gg 1$, when a noticeable increase of the total volume is expected. In this case the terms containing the inverse power of R in Eq. (21) may be neglected and it reduces in dimensionless units to

$$\hat{R}\ddot{\hat{R}} + \tfrac{3}{2}\dot{\hat{R}}^2 = 1, \tag{30}$$

where $\hat{R} \equiv R/R_\mathrm{cr}$ is the dimensionless radius and $\hat{t} = t/\tau_0$, with $\tau_0 = \sqrt{R_\mathrm{cr}^3\rho_\mathrm{w}/2\sigma}$, is the dimensionless time.

The asymptotic solution to this equation for $\hat{t} = t/\tau_0 \gg 1$ has the form $\hat{R} = \hat{a}\hat{t}^{\beta}$ with $\hat{a} = \sqrt{2/3}$ and $\beta = 1$, which reads in the dimensional variables

$$R(t) = at, \quad a \equiv \sqrt{\frac{4\sigma}{3R_\mathrm{cr}\rho_\mathrm{w}}}. \tag{31}$$

The last equation yields, together with Eq. (26), the velocity of the topmost part of the liquid in the slits for the condition $R(t) \gg R_\mathrm{cr}$,

$$u_0(t) = \tfrac{4}{3}\pi L_0\gamma a^3 t^3, \tag{32}$$

with the constant a from Eq. (31). The simple time dependence of $R(t)$, as it follows from Eq. (31) allows to find from Eq. (28) the percolation time,

$$t_\mathrm{p} = (\gamma\pi a^3/3)^{-1/4}, \tag{33}$$

and eventually the maximal velocity of water droplets,

$$u_\mathrm{max} = 4L_0\left(\frac{\pi a^3\gamma}{3}\right)^{1/4}. \tag{34}$$

The presented analysis remains valid in both cases of $T > T_\mathrm{t.p.}$ and $T < T_\mathrm{t.p.}$ provided the arising solid phase does not hinder the growth of vapor bubbles. Although this is not obvious, we assume that this is the case and leave the detailed analysis for future studies.

For a numerical estimate we use $\sigma = 0.07\,\mathrm{N/m}$, $\rho_w = 10^3\,\mathrm{kg/m^3}$, $\rho_{ice} = 917\,\mathrm{kg/m^3}$, $\eta = 10^{-3}\,\mathrm{N\,s/m^2}$ (as average values for plausible temperatures) and Eq. (10) for $\Delta\mu$. The phenomenological coefficient $q = 0.499999930$ in accordance with (Delale et al., 2003b) has been taken. This gives velocities exceeding meters per second only at a temperature higher than 450 K and for external pressures larger than 2.8 MPa, which corresponds to a height of the ice shell exceeding 30 km. Hence, in accordance with the kinetic theory of explosive boiling developed here, the water droplets would have too low a velocity for the plausible range of temperatures and pressures to explain the properties of the plume.

It is worth to add a few critical comments on the applicability of the kinetic approach. First, the range of validity of the modified homogeneous nucleation theory is not known at present. Hence we cannot judge the accuracy of the estimates for the maximal velocity u_{max}, obtained in the kinetic theory of explosive boiling. Still, we believe that this approach may be used to make accurate estimates for u_{max}, provided a solid and reliable theory for the nucleation rate γ is available. Second, the percolation time and the respective maximal velocity, computed here, refer only to the homogeneous nucleation in *pure* metastable water. We cannot exclude that other processes, like e.g. heterogeneous nucleation on impurities present in water, would give a much shorter percolation time and correspondingly a much larger maximal velocity. Presently, however, we do not possess any information about such impurities. On the other hand the explosive boiling not driven by dissolved gases, since the possible gases, such as CO_2, N_2 or CH_4, are not solvable in water at pressures of interest.

The current understanding of the kinetic theory of boiling does not allow to make a definite conclusion about the failure of the Cold Faithful model. In contrast, the thermodynamic approach presented here is not based on the homogeneous nucleation theory. It uses fundamental thermodynamic laws and hence should give a robust estimate for the upper limit of the maximal velocity u_{max}. The small value deduced for this quantity clearly indicate quantitative difficulties of the Cold Faithful model, which assumes shallow liquid water at the water triple point under the ice shell.

3. Analysis of the "Frigid Faithful" model

The "Frigid Faithful" model assumes the existence of a clathrate-rich ice layer deep below the south-polar ice cap (Kieffer et al., 2006; Gioia et al., 2007). Clathrates are stable only at high pressures, and thus, the cracks which connect the clathrate shell with the surface must be deep. In the deep cracks, however, the particles, produced by the decomposition of clathrates, will unavoidably collide with the cracks wells, on their way up to the surface. Such collisions decelerate the particles, and if they are not repeatedly re-accelerated by the gas stream, they cannot reach the surface. As a result, the particles leave the cracks at a speed that does not depend on the process of their production. Instead, the speed of the grains ejected from the cracks is settled by the subsurface dynamics of the gas and grains. Although the thermodynamic analysis of the explosive clathrate decomposition may be performed similarly to that of the explosive boiling, that is, using the thermodynamic relation (3) and the percolation condition (2), we will address here only the kinetics of particles in the gas stream. Based on the kinetics analysis, we show that the assumption of low-temperature clathrate decomposition leads to a problem with the subsurface transport of ice grains that eventually form the plume.

We start from the equation of motion for ice particles in a gas stream,

$$M_{grain}\frac{\mathrm{d}u_{grain}}{\mathrm{d}t} = b\pi R^2 \rho_{gas}\langle w_g\rangle(u_{gas} - u_{grain}), \tag{35}$$

which can be derived from gas-kinetic theory (Schmidt et al., 2008). Here u_{grain}, R and $M_{grain} = (\frac{4}{3})\pi R^3 \rho_{grain}$ are, respectively, the velocity, radius and mass of the grain, ρ_{grain} is the grains density, equal to the ice density. The coefficient $b = \frac{4}{3} + (1-\beta)\pi/6$ depends on the condensation coefficient β, which ranges from 0.1 to 1 (Shaw and Lamb, 1999; Batista et al., 2005) and quantifies the adsorption of water molecules by the icy grains. Finally, $\langle w_g\rangle = (8k_B T/\,\pi m_0)^{1/2}$ is the average molecular speed and u_{gas} is the speed of the gas. A similar equation has been derived by Gombosi and Horanyi (1986) for $\beta = 0$.

Let the collision of ice particles with the channel walls be a random Poisson process, that is, we assume that the probability to collide with a wall during an infinitesimal time interval $\mathrm{d}t$ is $\mathrm{d}t/\tau$, where τ is the average time between successive collisions. Let us introduce the corresponding collision length, which we define as $L_{coll} = u_{gas}\tau$. Then, $\exp[-t/(L_{coll}/u_{gas})]$ gives the probability that no collision has occurred during a time interval $(0, t)$. We also assume that in a wall collision the particles' velocity vanishes[2] and between collisions their dynamics is subject to Eq. (35). Hence the velocity of a grain at the outlet is completely determined by the time interval between its last wall collision and the instant when the particle leaves the channel. It also follows from this equation that for a fixed grain size only the gas density, speed and temperature near the outlet matter for the velocity distribution.

Referring to Schmidt et al. (2008) for details of the derivation, we give here the final result for the velocity distribution of particles

$$P(u_{grain}) = \frac{R}{R_*}\left[1 + \frac{R}{R_*}\right]\frac{u_{grain}}{u_{gas}}\left[1 - \frac{u_{grain}}{u_{gas}}\right]^{R/R_* - 1}. \tag{36}$$

[2]This assumption, which allows to develop an analytical theory is not very restrictive, since a more general model yields practically the same result, see Fig. 4.

Here $u_{\rm grain}$ is the velocity of a grain, $u_{\rm gas}$ is the gas velocity at the outlet, R is the particle radius, and R_* is defined as

$$R_* \equiv \frac{\rho_{\rm gas}}{\rho_{\rm grain}} \langle w_{\rm g}\rangle \left[1+\frac{\pi}{8}(1-\beta)\right]\frac{L_{\rm coll}}{u_{\rm gas}} = \omega\rho_{\rm gas}(T)\sqrt{T}\frac{L_{\rm coll}}{u_{\rm gas}}. \tag{37}$$

In this equation the critical radius R_* separates between slow big particles, with $R>R_*$, and small fast particles, with $R<R_*$. The latter move almost with the gas speed. Solutions of Eq. (36) are shown in Fig. 4 for $R=2\,\mu{\rm m}>R_*$ (left panel) and $R=0.2\,\mu{\rm m}$ (right panel) and compared to results from a Monte Carlo simulation of the Poisson process. In the figure we also show the results of the Monte Carlo simulation for a more general collision model, when a particle velocity after a wall collision is a random quantity from the interval $(0, r\,v_{\rm PRE})$, where $r<1$ and $v_{\rm PRE}$ is the pre-collisional velocity. As it follows from the figure, the generalized model yields practically the same results as the more simple model, which allows the analytical treatment.

The average velocity of particles of given size reads

$$\langle u_{\rm grain}\rangle = \left(1+\frac{R}{2R_*}\right)^{-1} u_{\rm gas}. \tag{38}$$

Thus, the velocity of large particles decays with their size as $\langle u_{\rm grain}(R)\rangle \sim 1/R$.

Using Eqs. (37) and (38) one can relate the characteristic collision length and the gas temperature,

$$L_{\rm coll} = \frac{R}{2\omega\rho_{\rm gas}(T)\sqrt{T}(\langle u_{\rm grain}\rangle^{-1} - u_{\rm gas}^{-1})}, \tag{39}$$

where the coefficient ω is defined in Eq. (37). The last equation illustrates the dependence of the collision length, which is consistent with given particle radius, average velocity and the gas speed, on the gas temperature. Using $\langle u_{\rm grain}\rangle = 100\,{\rm m/s}$, which may be deduced from the brightness gradient of the plume (Ingersoll et al., 2006; Schmidt et al., 2008), $u_{\rm gas} = 500\,{\rm m/s}$ (Hansen et al., 2006; Tian et al., 2007) and density of saturated vapor at temperature T for $\rho_{\rm gas}(T) = \rho_{\rm v}^{\rm s.g.}(T)$, we calculate $L_{\rm coll}$ for particles in the micron-size range.

Results are shown in Fig. 5. For vapor temperatures as low as 140 K, assumed in the Frigid Faithful model (Kieffer et al., 2006; Gioia et al., 2007), the equilibrium vapor density is very small. In this case the gas cannot efficiently accelerate micron-sized grains, which results in an extremely large collision length in our model (larger than 100 km). This requires either implausibly wide or straight channels or cracks. Vice versa, more realistic cracks, curved and irregular in shape, would lead for such a dilute gas to a very small flux of grains, too small to create a visible dust plume.

At larger temperatures the gas can transport more and more grains. In this case, the repeated wall collisions provide an effective friction process, decelerating the grains

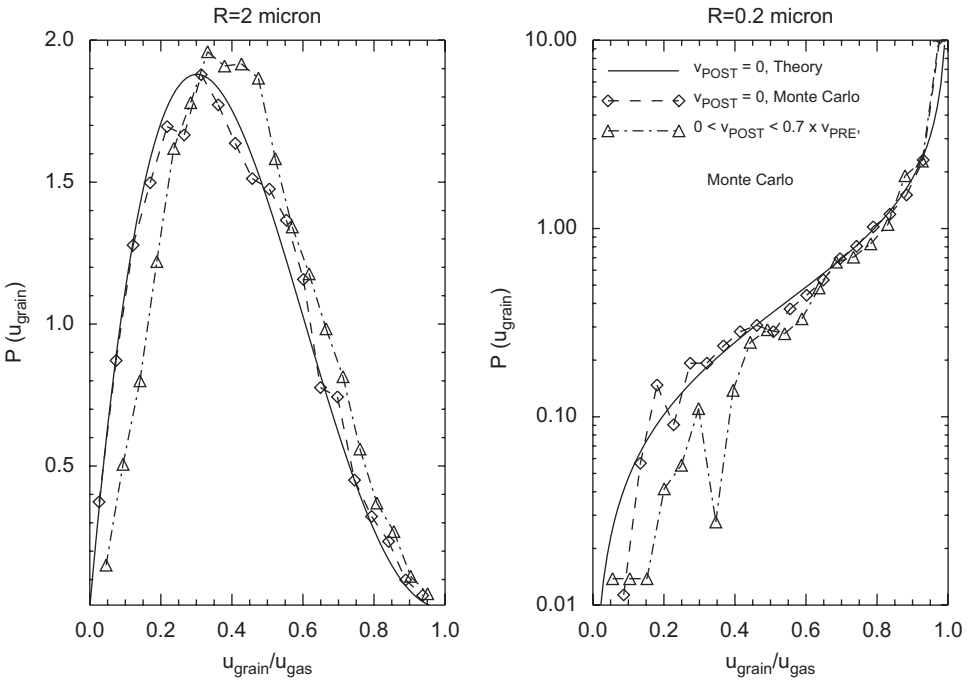

Fig. 4. Solutions of Eq. (36) (solid curves) for $R=2\,\mu{\rm m}>R_*\approx 0.6\,\mu{\rm m}$ (left panel) and $R=0.2\,\mu{\rm m}$ (right panel). Here, $T=234.14\,{\rm K}$, $\rho_{\rm gas}=0.00305\,{\rm kg/m^3}$, and $u_{\rm gas}=379.4\,{\rm m/s}$, which follow from a model of water vapor expanding from triple point conditions through a straight channel to vacuum (Brilliantov et al., 2007). Further parameters are $\beta=0.2$ and $L_{\rm col}=0.1\,{\rm m}$ (Schmidt et al., 2008). Results from a Monte Carlo simulation of the stochastic model for wall impacts are shown as diamond symbols. Also shown are results from Monte Carlo simulations where the post-collisional speed of particles, after a wall impact, is not reduced to zero (triangles). In this case the post-collisional speed $v_{\rm POST}$ was randomly assigned a value in the interval $[0, 0.7v_{\rm PRE}]$, in terms of the pre-collisional speed $v_{\rm PRE}$.

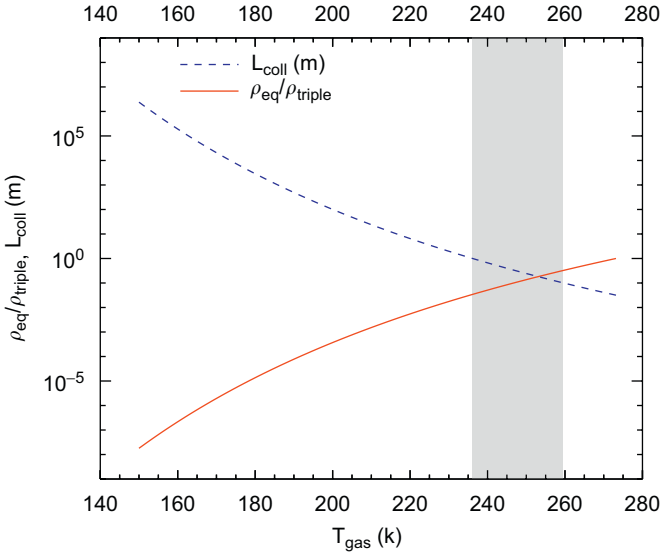

Fig. 5. Collision length as a function of vapor temperature for micron-size particles. For $\rho_{gas}(T)$ the density of saturated vapor $\rho_v^{s.g.}(T)$ at temperature T is taken from the relation, $\rho_v^{s.g.}(T) = p_v^{s.g.}(T)m_0/k_B T$, where $p_v^{s.g.}(T)$ is given by the empirical Eq. (19).

relative to the gas. This mechanism explains the speed differences of water vapor and dust grains in the plume (Schmidt et al., 2008). Detailed modeling and comparison to the observed brightness gradient of the dust plumes suggests collision lengths, and thus crack widths, on the order of 10 cm (Schmidt et al., 2008). The range of gas temperatures that follows for collision lengths between centimeters and meters is about 240–260 K (indicated in Fig. 5 by the gray-shaded area). Since the gas temperature drops by a few tens of degrees when it expands from the site of evaporation (Brilliantov et al., 2007; Schmidt et al., 2008), the actual temperatures there must be near the melting point. At such high-temperatures clathrates would not be stable, unless they are subjected to extremely high pressure, which would be difficult to understand within the present knowledge about the satellite.

4. Conclusion

We performed quantitative estimates for two recent qualitative models of the Enceladus plume—the "Cold Faithful" and "Frigid Faithful" models. Namely, we compute the velocities of the dust particles, expected for these models, and compare them with the velocities inferred from the Cassini data.

Analyzing the process of an explosive boiling due to a sudden pressure drop, as it is assumed in the Cold Faithful model, we formulate the condition of explosive boiling. In this case the coalescence of nucleating and growing in liquid vapor bubbles must occur much faster than the buoyancy driven motion of the bubbles. Moreover, we argue that the maximal kinetic energy, which expanding liquid acquires, is achieved at the percolation point of the gaseous phase. Beyond this point the vapor can find pathways through liquid to the surface and escape it without carrying the liquid along. We consider in detail two different scenarios—boiling accompanied by freezing and boiling without freezing.

To estimate the maximal velocity of the water droplets produced in the explosive boiling, which later freeze and form icy grains, we develop two approaches—the thermodynamic theory and the kinetic one. The former approach uses the relation between the maximal reversible work and the change of the Gibbs free energy in a phase transformation. It gives the upper limit for the kinetic energy of particles produced in the explosive boiling, which follows from the basic thermodynamic equations. In the latter approach the microscopic kinetics of the nucleation of vapor bubbles and their growth is analyzed. It uses the phenomenological modification of the classical nucleation theory (CNT). This is the most convenient analytical tool, available in the scientific literature, designed to overcome the deficiency of the CNT at low temperatures. Unfortunately, the range of validity of this modified theory is not presently known. Both, kinetic and thermodynamic theories predict velocities of dust particles that are much smaller than those inferred from the Cassini data.

Analyzing the Cold Faithful model we focused on the explosive boiling, which is expected to give the main contribution to the particles speed. It is also interesting to estimate the speed of the water column streaming upwards in a suddenly opened crack due to the hydrodynamic pressure from the ice shell of height H. For the height of the water column in a crack (measured from the bottom) one can derive the equation

$$\frac{d}{d\hat{t}}(\hat{h}\dot{\hat{h}}) = 1 - \delta\dot{\hat{h}} - \hat{h},$$

written for the dimensionless height, $\hat{h} = h/h_0$ and time, $\hat{t} = t/t_0$.

Here $h_0 = (\rho_{ice}/\rho_w)H$, $t_0 = (\rho_{ice}H/\rho_w g)^{1/2}$ and $\delta \ll 1$ is the friction coefficient, due to the water viscosity. The water column relaxes to the equilibrium height h_0 with the characteristic velocity $u_{hyd} \sim h_0/t_0 \sim \sqrt{gH}$. For a reasonable maximal height of the ice shell, $H < 10^4$ m, the characteristic velocity is about 30 m/s. Therefore, even if the hydrodynamic velocity u_{hyd} and u_{max} due to the explosive boiling sum up, the resulting velocity of the particles is still much smaller than Enceladus' escape speed. Thus mean ejection speeds on the order of the escape speed, and slightly below, necessary to build the large plume of ice grains observed at Enceladus, are difficult to understand from the Cold Faithful model.

In the framework of the Frigid Faithful model the dust plume is formed by ice grains produced in an explosive decomposition of clathrates. These are lifted then up by the gas flowing through the cracks in the ice shell. The gas is also the product of the decomposition, which takes place deeply under the surface. We analyze the particle motion and argue that for deep cracks the collisions of particles with the cracks' walls are unavoidable and propose a model

of random wall collisions. We study analytically a simplified collision model and perform Monte Carlo simulations for a more general model. We find the velocity distribution of grains and observe that the simplified model provides a good approximation of the more general one. The average particle velocity is obtained as a function of the gas density, gas velocity and cracks' width. We show that for gas temperatures around 140 K, the gas is too dilute to accelerate micron-sized grains to a mean speed of $\sim$100 m/s consistent with observations: it would require a collision length larger than 100 km, which is not realistic for the small moon Enceladus (250 km radius). On the other hand, for a reasonable crack width of $0.1-1$ m, leading to the observed gas speeds and fluxes (Schmidt et al., 2008), the gas (vapor) density corresponding to temperatures of liquid water is expected. Hence we conclude that the Frigid Faithful model with clathrate reservoir temperatures around 140 K cannot explain the existence of Enceladus dust plume and its structure.

References

Alehossein, H., Quin, Z., 2007. Numerical analysis of Rayleigh Plesset equation for cavitating water jets. Int. J. Numer. Methods Eng. 72, 780807.

Batista, E.R., Ayotte, P., Bilic, A., Kay, B., Jonsson, H., 2005. What determines the sticking probability of water molecule on ice? Phys. Rev. Lett. 95, 223201.

Blander, M., Katz, J.L., 1975. Bubble nucleation in liquids. AIChE J. 21, 833–848.

Brennen, C.E., 1995. Cavitation and Bubble Dynamics. Oxford University Press, New York.

Brilliantov, N.V., Schmidt, J., Spahn, F., 2007. Nucleation and growth of a solid phase in a gas expanding into vacuum. Int. J. Mod. Phys. C 18, 676–684.

Collins, G.C., Goodman, J.C., 2007. Enceladus' south polar sea. Icarus 189, 72–82.

De Pater, I., Showalter, M.R., Lissauer, J.J., Graham, J.R., 1996. Keck infrared observations of Saturn's E and G rings during Earth's 1995 ring plane crossings. Icarus 121, 195–198.

De Pater, I., Martin, S., Showalter, M.R., 2004. Keck infrared observations of Saturn's E and G rings during Earth's ring plane crossings in August 1995. Icarus 172, 446.

Debenedetti, P.G., 1996. Metastable Liquids: Concepts and Principles. Princeton University Press, Princeton, NJ.

Delale, C.F., Hruby, J., Marsik, F., 2003a. Homogeneous bubble nucleation in liquids: the classical theory revisited. J. Chem. Phys. 118, 792–806.

Delale, C.F., Okita, K., Y.M., 2003b. Steady-state cavitating nozzle flows with nucleation. In: Fifth International Symposium on Cavitation, Osaka, Japan, November 1–4, Cav03-GS-4:1–8.

Dougherty, M.K., Khurana, K.K., Neubauer, F.M., Russell, C.T., Saur, J., Leisner, J.S., Burton, M.E., 2006. Identification of a dynamic atmosphere at Enceladus with the Cassini magnetometer. Science 311, 1406–1409.

Gioia, G., Chakraborty, P., Marshak, S., Kieffer, S.W., 2007. Unified model of tectonics and heat transport in a Frigid Enceladus. Proc. Natl. Acad. Sci. 104, 13578–13591.

Gombosi, T.I., Horanyi, M., 1986. Time-dependent numerical modeling of dust halo formation at comets. Astrophys. J. 311, 491–500.

Grimmett, G., 1989. Percolation. Springer, New York.

Haff, P.K., Eviatar, A., Siscoe, G., 1983. Ring and plasma: the enigmae of Enceladus. Icarus 56, 426–438.

Hansen, C.J., Esposito, L., Stewart, A.I.F., Colwell, J., Hendrix, A., Pryor, W., Shemansky, D., West, R., 2006. Enceladus' water vapor plume. Science 311, 1422–1425.

Horányi, M., Burns, J.A., Hamilton, D.P., 1992. The dynamics of Saturn's E ring particles. Icarus 97, 248–259.

Ingersoll, A.P., Porco, C.C., Helfenstein, P., West, R.A., Cassini ISS Team, 2006. Models of the Enceladus plumes. In: Bulletin of the American Astronomical Society, vol. 38, p. 508.

Juhász, A., Horányi, M., 2002. Saturn's E ring: a dynamical approach. J. Geophys. Res. (Space Phys.) 107, 1.

Kagan, Y., 1960. The kinetics of boiling of pure liquids. Russ. J. Phys. Chem. 34, 42–46.

Kieffer, S.W., Lu, X., Bethke, C.M., Spencer, J.R., Marshak, S., Navrotsky, A., 2006. A clathrate reservoir hypothesis for Enceladus' south polar plume. Science 314, 1764.

Landau, L.D., Lifshitz, E.M., 1980. Statistical Physics Part 1, third ed. Butterworth-Heinemann, Oxford.

Lemmon, E.W., McLinden, M.O., Friend, D., 2005. Thermophysical properties of fluid systems. In: Linstrom, P.E., Mallard, W. (Eds.), NIST Chemistry WebBook, NIST Standard Reference Database Number 69. National Institute of Standards and Technology, Gaithersburg, MD.

Li, J., Peterson, G.P., Chieng, P., 2005. Mechanical nonequilibrium consideration in homogeneous bubble nucleation for unsteady-state boiling. Heat Mass Transfer 48, 3081–3096.

Lorenz, R.D., 2002. Thermodynamics of geysers: application to Titan. Icarus 156, 176–183.

Lubetkin, S.D., 2003. Why is it much easier to nucleate gas bubbles than theory predicts? Langmuir 19, 2575–2587.

Matson, D.L., Castillo, J.C., Lunine, J., Johnson, T.V., 2007. Enceladus' plume: compositional evidence for a hot interior. Icarus 187, 569–573.

Nicholson, P.D., Showalter, M.R., Dones, L., French, R.G., Larson, S.M., Lissauer, J.J., McGhee, C.A., Sicardy, B., Seitzer, P., Danielson, G.E., 1996. Observations of Saturn's ring-plane crossing in August and November 1995. Science 272, 509–516.

Peeters, P., Gielis, J.J.H., van Dongen, M.E.H., 2002. The nucleation behavior of supercooled water vapor in helium. J. Chem. Phys. 117 (12), 5647–5653.

Plesset, M.S., Prosperetti, A., 1977. Bubble dynamics and cavitation. Annu. Rev. Fluid Mech. 9, 145–185.

Porco, C.C., Helfenstein, P., Thomas, P.C., Ingersoll, A.P., Wisdom, J., West, R., Neukum, G., Denk, T., Wagner, R., Roatsch, T., Kieffer, S., Turtle, E., McEwen, A., Johnson, T.V., Rathbun, J., Veverka, J., Wilson, D., Perry, J., Spitale, J., Brahic, A., Burns, J.A., DelGenio, A.D., Dones, L., Murray, C.D., Squyres, S., 2006. Cassini observes the active south pole of Enceladus. Science 311, 1393–1401.

Schmidt, J., Brilliantov, N.V., Spahn, F., Kempf, S., 2008. Formation of Enceladus dust plume. Nature 451, 685.

Shaw, R.A., Lamb, D., 1999. Experimental determination of the thermal accommodation and condensation coefficients of water. J. Chem. Phys. 111, 10659–10663.

Showalter, M., Cuzzi, J., Larson, S., 1991. Structure and particle properties of Saturn's E ring. Icarus 94, 451–473.

Spahn, F., Schmidt, J., Albers, N., Hörning, M., Makuch, M., Seiß, M., Kempf, S., Srama, R., Dikarev, V., Helfert, S., Moragas-Klostermeyer, G., Krivov, A.V., Sremčević, M., Tuzzolino, A.J., Economou, T., Grün, E., 2006. Cassini dust measurements at Enceladus and implications for the origin of the E ring. Science 311, 1416–1418.

Spencer, J.R., Pearl, J.C., Segura, M., Flasar, F.M., Mamoutkine, A., Romani, P., Buratti, B.J., Hendrix, A.R., Spilker, L.J., Lopes, R.M.C., 2006. Cassini encounters Enceladus: background and the discovery of a south polar hot spot. Science 311, 1401–1405.

Spitale, J.N., Porco, C.C., 2007. Association of the jets of Enceladus with the warmest regions on its south-polar fractures. Nature 449, 695–697.

Tian, F., Stewart, A.I.F., Owen, B.T., Larsen, K.M., Esposito, L.W., 2007. Monte Carlo simulations of the water vapor plumes on Enceladus. Icarus 188, 154–161.

Waite, J.H., Combi, M.R., Ip, W.-H., Cravens, T.E., McNutt, R.L., Kasprzak, W., Yelle, R., Luhmann, J., Niemann, H., Gell, D., Magee, B., Fletcher, G., Lunine, J., Tseng, W.-L., 2006. Cassini ion and neutral mass spectrometer: Enceladus plume composition and structure. Science 311, 1419–1422.

Zettlemoyer, A.C., 1969. Nucleation. Dekker, New York.